Research Article | Vol. 25, No. 6 | 20 Mar 2017 | OPTICS EXPRESS 5972

Optics EXPRESS

# Low threshold optical bistability in one-dimensional gratings based on graphene plasmonics

JUN GUO, LEYONG JIANG, YUE JIA, XIAOYU DAI, YUANJIANG XIANG,* AND DIANYUAN FAN

*SZU-NUS Collaborative Innovation Center for Optoelectronic Science and Technology, Key Laboratory of Optoelectronic Devices and Systems of Ministry of Education and Guangdong Province, College of Optoelectronic Engineering, Shenzhen University, Shenzhen 518060, China*
*xiangyuanjiang@126.com

**Abstract:** Optical bistability of graphene surface plasmon is investigated numerically, using grating coupling method at normal light incidence. The linear surface plasmon resonance is strongly dependent on Femi-level of graphene, hence it can be tuned in a large wavelength range. Due to the field enhancement of graphene surface plasmon resonance and large third-order nonlinear response of graphene, a low-threshold optical hysteresis has been observed. The threshold value with 20MW/cm$^2$ and response time with 1.7ps have been verified. Especially, it is found that this optical bistability phenomenon is angular insensitivity for near 15° incident angle. The threshold of optical bistability can be further lowered to 0.5MW/cm$^2$ by using graphene nanoribbons, and the response time is also shorten to 800fs. We believe that our results will find potential applications in bistable devices and all-optical switching from mid-IR to THz range.



**OCIS codes:** (190.1450) Bistability; (240.6680) Surface plasmons; (050.2770) Gratings; (160.2100) Electro-optical materials.

## References and links

1. R. W. Boyd, *Nonlinear Optics* (Academic, 1992).
2. D. A. Mazurenko, R. Kerst, J. I. Dijkhuis, A. V. Akimov, V. G. Golubev, D. A. Kurdyukov, A. B. Pevtsov, and A. V. Selkin, "Ultrafast optical switching in three-dimensional photonic crystals," Phys. Rev. Lett. **91**(21), 213903 (2003).
3. G. Assanto, Z. Wang, D. J. Hagan, and E. W. VanStryland, "All-optical modulation via nonlinear cascading in type II second-harmonic generation," Appl. Phys. Lett. **67**(15), 2120–2122 (1995).
4. H. Nihei, and A. Okamoto, "Photonic crystal systems for high-speed optical memory device on an atomic scale," Proc. SPIE **4416**, 470–473 (2001).
5. J. Leuthold, C. Koos, and W. Freude, "Nonlinear silicon photonics," Nature Photonics **4**(8), 535–544 (2010).
6. D. J. Moss, R. Morandotti, A. L. Gaeta, and M. Lipson, "New cmos-compatible platforms based on silicon nitride and hydex for nonlinear optics," Nature Photonics **7**(8), 597–607 (2013).
7. V. G. Taeed, N. J. Baker, L. Fu, K. Finsterbusch, M. R. Lamont, D. J. Moss, H. C. Nguyen, B. J. Eggleton, D. Y. Choi, S. Madden, and B. Luther-Davies, "Ultrafast all-optical chalcogenide glass photonic circuits," Opt. Express **15**(15), 9205–9221 (2007).
8. F. S. Felber, and J. H. Marburger, "Theory of nonresonant multistable optical devices," Appl. Phys. Lett. **28**(12), 731–733 (1976).
9. M. Soljacic, M. Ibanescu, S. G. Johnson, Y. Fink, and J. D. Joannopoulos, "Optimal bistable switching in nonlinearphotonic crystals," Phys. Rev. E **66**(5), 055601 (2002).
10. S. F. Mingaleev, and Y. S. Kivshar, "Nonlinear transmission and light localization in photonic-crystalwaveguides," J. Opt. Soc. Am. B **19**(9), 2241 (2002).
11. Q. M. Ngo, S. Kim, S. H. Song, and R. Magnusson, "Optical bistable devices based on guided-mode resonance in slab waveguide gratings," Opt. Express **17**(26), 23459–23467 (2009).
12. P. Vincent, N. Paraire, M. Neviere, A. Koster, and R. Reinisch, "Grating in nonlinear optics and optical bistability," J. Opt. Soc. Am. B **2**(7), 1106–1116 (1985)
13. G. M. Wysin, H. J. Simon, and R. T. Deck, "Optical bistability with surface plasmons," Opt. Lett. **6**, 30-32 (1981).
14. C. Min, P. Wang, C. Chen, Y. Deng, Y. Lu, H. Ming, T. Ning, Y. Zhou, and G. Yang, "All-optical switching in subwavelength metallic grating structure containing nonlinear optical materials," Opt. Lett. **33**(8), 869–871 (2008).

#284595 https://doi.org/10.1364/OE.25.005972
Journal © 2017 Received 12 Jan 2017; revised 27 Feb 2017; accepted 1 Mar 2017; published 6 Mar 2017

Optics EXPRESS

15. S. Tang, B. Zhu, S. Xiao, J. Shen, and L. Zhou, "Low-threshold optical bistabilities in ultrathin nonlinear metamaterials," Opt. Lett. **39**(11), 3212–3215 (2014).
16. G. A. Wurtz, R. Pollard, and A. V. Zayats, "Optical bistability in nonlinear surface-plasmon polaritonic crystals," Phys. Rev. Lett. **97**(5), 057402 (2006).
17. F. H. L. Koppens, D. E. Chang, and F. J. Garcia de Abajo, "Graphene plasmonics: a platform for strong light matter interactions," Nano Lett. **11**(8), 3370–3377 (2011).
18. Q. Bao, and K. P. Loh, "Graphene photonics, plasmonics, and broadband optoelectronic devices," ACS nano **6**(5), 3677–3694 (2012).
19. A. N. Grigorenko, M. Polini, and K. S. Novoselov, "Graphene plasmonics," Nat. Photonics **6**(11), 749–758 (2012).
20. K. S. Novoselov, A. K. Geim, S. V. Morozov, D. Jiang, Y. Zhang, S. V. Dubonos, I. V. Grigorieva, and A. A. Firsov, "Electric feld effect in atomically thin carbon flms," Science **306**(5696), 666–669 (2004).
21. A. H. Castro Neto, F. Guinea, N. M. R. Peres, K. S. Novoselov, and A. K. Geim, "The electronic properties of graphene," Rev. Mod. Phys. **81**(1), 109–162 (2009).
22. M. Liu, X. Yin, E. Ulin-Avila, B. Geng, T. Zentgraf, L. Ju, F. Wang, and X. Zhang, "A graphene-based broadband optical modulator," Nature **474**(7349), 64–67 (2011).
23. F. Bonaccorso, Z. Sun, T. Hasan, and A. C. Ferrari, "Graphene photonics and optoelectronics," Nat. Photonics **4**(9), 611–622 (2010).
24. C. H. Liu, Y. C. Chang, T. B. Norris, and Z. Zhong, "Graphene photodetectors with ultra-broadband and high responsivity at room temperature," Nat. Nanotech. **9**(4), 273–278 (2014).
25. Q. Bao, H. Zhang, B. Wang, Z. Ni, C. H. Y. X. Lim, Y. Wang, D. Y. Tang, and K. P. Loh, "Broadband graphene polarizer," Nat. Photonics **5**(7), 411–415 (2011).
26. H. Zhang, S. Virally, Q. Bao, K. P. Loh, S. Massar, N. Godbout, and P. Kockaert, "Z-scan measurement of the nonlinear refractive index of graphene," Opt. Lett. **37**(11), 1856–1858 (2012).
27. N. M. R. Peres, Yu. V. Bludov, J. E. Santos, A. P. Jauho, and M. I. Vasilevskiy, "Optical bistability of graphene in the terahertz range," Phys. Rev. B **90**(12), 125425 (2014)
28. E. Hendry, P. J. Hale, J. Moger, A. K. Savchenko, and S. A. Mikhailov, "Coherent nonlinear optical response of graphene," Phys. Rev. Lett. **105**(9), 097401 (2010).
29. A. E. Nikolaenko, N. Papasimakis, E. Atmatzakis, Z. Luo, Z. X. Shen, F. D. Angelis, S. A. Boden, E. D. Fabrizio, and N. I. Zheludev, "Nonlinear graphene metamaterial," Appl. Phys. Lett. **100**(18), 181109 (2012).
30. X. Dai, L. Jiang, and Y. Xiang, "Low threshold optical bistability at terahertz frequencies with graphene surface plasmon," Sci. Rep. **5**, 12271 (2015).
31. T. Christensen, W. Yan, A. Jauho, M. Wubs, and N. A. Mortensen, "Kerr nonlinearity and plasmonic bistability in graphene nanoribbons," Phys. Rev. B **92**, 121407(R) (2015).
32. T. Christopoulos, O. Tsilipakos, N. Grivas, and E. E. Kriezis, "Coupled-mode-theory framework for nonlinear resonators comprising graphene," Phys. Rev. E **94**, 062219 (2016).
33. C. Horvath, D. Bachman, R. Indoe, and V. Van, "Photothermal nonlinearity and optical bistability in a graphene–silicon waveguide resonator," Opt. Lett. **38**(23), 5036–5039 (2013).
34. Q. Bao, J. Chen, Y. Xiang, K. Zhang, S. Li, X. Jiang, Q. H. Xu, K. P. Loh, and T. Venkatesan, "Graphene nanobubbles: a new optical nonlinear material," Adv. Opt. Mater. 3(6), 744–749 (2015).
35. W. Gao, J. Shu, C. Qiu, and Q. Xu, "Excitation of plasmonic waves in graphene by guided-mode resonances," ACS nano **6**(9), 7806–7813 (2012).
36. T. R. Zhan, F. Y. Zhao, X. H. Hu, X. H. Liu, and J. Zi, "Band structure of plasmons and optical absorption enhancement in graphene on subwavelength dielectric gratings at infrared frequencies," Phys. Rev. B **86**(16), 165416 (2012).
37. P. Y. Chen, and A. Alu, "Atomically thin surface cloak using graphene monolayers," ACS Nano **5**(7), 5855–5863 (2011).
38. G. W. Hanson, "Dyadic Green's functions and guided surface waves for a surface conductivity model of graphene," J. Appl. Phys. **103**(6), 064302 (2008).
39. C. R. Dean, A. F. Young, I. Meric, C. Lee, L. Wang, S. Sorgenfrei, K. Watanabe, T. Taniguchi, P. Kim, K. L. Shepard, and J. Hone, "Boron nitride substrates for high-quality graphene electronics," Nat. Nanotechnol. **5**(10), 722–726 (2010).
40. K. Bolotin, K. Sikes, Z. Jiang, M. Klima, G. Fudenberg, J. Hone, P. Kim, and H. Stormer, "Ultrahigh electron mobility in suspended graphene," Solid State Commun. **146**(9), 351–355 (2008).
41. M. G. Moharam, E. B. Grann, and D. A. Pommet, "Formulation for stable and efficient implementation of the rigorous coupled-wave analysis of binary gratings," J. Opt. Soc. Am. A **12**(5), 1068–1076 (1995).
42. M. G. Moharam, D. A. Pommet, and E. B. Grann, "Stable implementation of the rigorous coupled-wave analysis for surface-relief gratings: enhanced transmittance matrix approach," J. Opt. Soc. Am. A **12**(5), 1077–1086 (1995).

## 1. Introduction

In nonlinear optical systems, particularly in some resonant optical structures, it is possible to have two stable output states for a given input state. This phenomenon is called optical bista-

Optics EXPRESS

bility [1]. Optical bistability has drawn a lot of attentions due to its potential applications in all-optical switching [2], optical transistor [3] and optical memory [4], which can be used for high-speed processing of optical signals. As a fundamental challenge, the threshold of optical bistability has to be lowered as much as possible. Optical bistability is a pure third-order nonlinear process, which stems from the intensity dependent refractive index of the nonlinear materials. However, most of the solid state materials have low nonlinear refractive index (or third-order susceptibility). As a result, optical bistability based on these materials has a very high threshold (~10GW/cm$^2$). It is difficult to generate such intense light, which may also damages the materials. There are two well-known ways to generate large nonlinear response. Except for using materials with large nonlinear susceptibility, one can achieve large near-filed intensity enhancement using delicate resonant structures. Enlarging the interaction length of light and nonlinear materials is also possible, however the device will become very bulky. Numerous nonlinear materials [5–7] and optical structures have been studied in the recent years to realize optical bistability. The most classical configuration is Fabry-Perot cavity filled with nonlinear materials [8]. Other structures like nonlinear photonic crystals [9, 10], guide-mode resonance [11, 12], and surface plasmons [13–16] (SPs) have also been widely studied. Especially for SPs of metal nanostructures, very large near field enhancement and confinement can be achieved, which usually results in stronger nonlinear effects and smaller device size. However, SPs of metals also suffer from large ohmic losses, narrow band response and the lack of tunability [17], which hinder their applications in all-optical devices.

On the other hand, doped graphene has emerged as an alternative, unique two-dimensional plasmonic material, which has lower ohmic loss, broadband response and high tunability [17–19]. In linear optics, graphene shows excellent optical and electrical characteristics [20–23] and becomes a good candidate for optoelectronic devices, such as optical modulators [22], photodetectors [24] and polarizers [25], etc. Additionally, graphene also exhibits large nonlinear susceptibility and ultra-fast nonlinear response [26–29]. Some efforts on graphene bistability have been done recently, using suspended graphene [27], graphene SPs [30–32] and other resonant structures, such as waveguide [33] and Fabry-Perot cavity [34]. However, either the threshold of graphene bistability is still high, or its operation bandwidth is limited in THz frequency.

Compared to other resonant structures, such as SPs of noble metals, the graphene SPs have much larger near-field enhancement and better confinement [17]. Therefore, bistable devices based on graphene SPs are expected to have a much lower threshold and high tunability. However, in order to utilize the graphene SPs, the excitation becomes a challenge. Due to their extraordinary confinement, the effective wavelength of graphene SPs is much smaller than vacuum light. To compensate the large phase mismatch, extra coupling methods like prism [30] or grating coupling [35, 36] are required. In shorter wavelength range, prism with higher refractive index or grating with smaller period should be used. This is the reason that most studies on graphene SPs are limited in THz range. Compared to prism coupling, where prism with high index and large incident angle are required, grating coupling is easier to implement in experiments at short wavelength range, especially at infrared wavelengths.

In this work, we study bistability of graphene SPs numerically, which is excited by grating coupling at mid-infrared wavelength. Combining the large field enhancement of SPs and large nonlinear response of graphene, we are able to get optical bistability with thresholds arround 20MW/cm$^2$. It is surprising that with such a short interaction length between light and graphene, a considerable nonlinear response can be achieved in the proposed structure. We also show bistability based on SPs of graphene nanoribbons, where grating is absent. In this case, an even lower threshold is realized (0.5MW/cm$^2$). We also show the effects of doping levels and inherent losses of the graphene. The time responses of bistability are discussed as well. According to our results, graphene SPs may have potential applications in tunable, compact, and low threshold optical bistable devices.

Optics EXPRESS

## 2. Theoretical models and methods

As shown in Fig. 1(a), the graphene is covered on a dielectric grating. At mid-infrared wavelengths, the substrate is chosen to be $CaF_2$ with $n_s = 1.3$. The grating ridge is Si with $n_r = 3.418$, and the groove is air. A transverse magnetic (TM) polarized light incident from the air to the proposed structure, this restriction is vital for graphene SPs with 1D grating coupling, while it can be overcome by using a 2D structure [36]. In this work, graphene SPs are utilized to get high near-field enhancement and a resonant optical feedback, which are necessary for low-threshold bistability. The period of grating is $\Lambda = 1\mu$m, with a ridge of $\Delta = 0.4\mu$m and a thickness of grating layer of $d = 0.1\mu$m. It is known that the complex linear surface conductivity of graphene is contributed by intraband and interband $\sigma_0 = \sigma_{intra} + \sigma_{inter}$ terms, and can be expressed according to the Kubo formula [37, 38]:

$$\sigma_{intra} = i\frac{e^2 k_B T}{\pi\hbar^2(\omega + i\Gamma)}\left[\frac{E_F}{k_B T} + 2\ln\left(e^{-\frac{E_F}{k_B T}} + 1\right)\right], \tag{1}$$

$$\sigma_{inter} = i\frac{e^2}{4\pi\hbar}\ln\left[\frac{2E_F - (\omega + i\Gamma)\hbar}{2E_F + (\omega + i\Gamma)\hbar}\right], \tag{2}$$

where $\omega$ is angular frequency, $E_F$ is Fermi energy, $\Gamma = 1/\tau$ is carrier scattering rate, $\tau$ is relaxation time, $T$ is absolute temperature of environment. In this work, the temperature $T = 300$K, Fermi energy $E_F$ can be tuned dynamically by electrostatic gating and $\tau$ is related to carrier mobility $\mu = ev_f^2\tau/E_F$, $v_f \approx 10^6$m/s is Fermi velocity. In the limit $\omega\tau \gg 1$ and ignoring the third harmonic generation, the third-order nonlinear surface conductivity can be expressed as [27, 30]:

$$\sigma_3 = -i\frac{9}{8}\frac{e^4 v_f^2}{\pi E_F \hbar^2 \omega^3}, \tag{3}$$

The negative imaginary $\sigma_3$ shows the self-focusing type nonlinear response of graphene. The linear and nonlinear response of the proposed structure are studied by calculating numerically using FEM method (Comsol Multiphysics). In the FEM method, graphene is modeled as a surface conductive sheet with zero thickness, and the total surface conductivity is $\sigma_g = N\sigma_0 + \sigma_3|E_x|^2$. The parameter $N$ is the layer number of few-layer graphene (FLG), with $N = 1$ for monolayer graphene (MLG). While MLG SPs have better confinement, it is more difficult to excite it at mid-infrared wavelength, because a small grating period is required. On the contrary, FLG SPs are easier to excite. Therefor, in the following studies, FLG with $N = 5$ is used. Note that the linear conductivity can not be superposed linearly for more than 6 layers, and for odd number layers of FLG, the nonlinear response is the same as that of MLG [27].

## 3. Results and discussions

Figure 1(c) shows the linear transmittance of graphene SPs under different $E_F$ in wavelength spectrum, where the light is normally incident and $\tau$ is fixed to be 400fs. Note that, in actual experiments, $E_F$ is also influenced by the substrates. In literatures, relaxation time of 1000fs have been reported [39, 40]. The strongest resonances are marked by arrows, correspond to the second stop band of graphene SPs with grating [36]. The phase matching condition $\beta = k_x + mK$ and $m = 1$ are fulfilled, where $\beta$ is the effective wave vector of graphene SPs, $k_x$ is the transverse wave vector of light (zero for normally incident), and $K = 2\pi/\Lambda$. Other weak resonances are results of higher order stop bands, i.e. $m > 1$. In the following discussions, only the strongest resonance is considered.

Similar to the results in [35], the linear resonant wavelengths can be tuned by varying $E_F$. As $E_F$ increases, the resonant wavelength decreases. In Fig. 1(c), the solid lines are calculated by scanning wavelengths in frequency domain using FEM method. To examine the accuracy of the

Optics EXPRESS

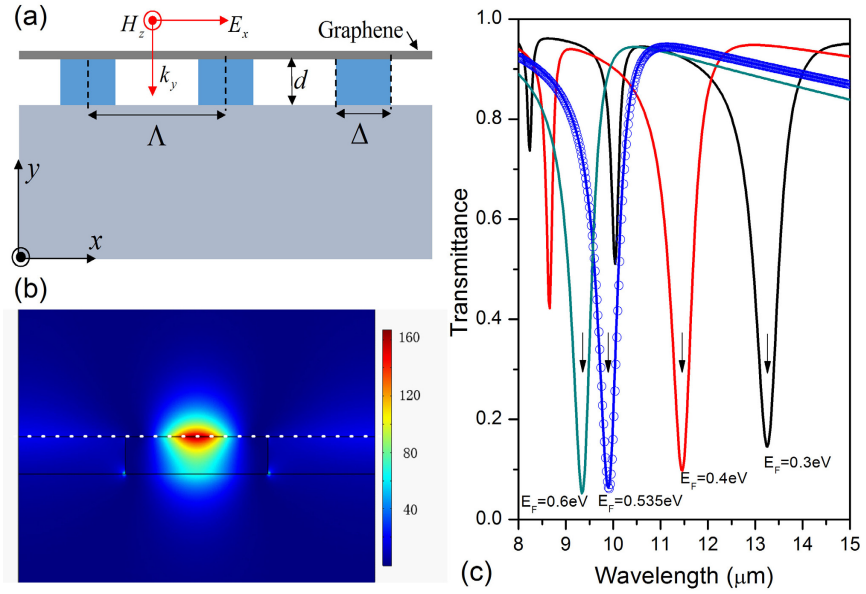


Fig. 1. (a) Schematic of the proposed structure. (b) Distribution of normalized electric filed intensity. (c) Linear transmittance in wavelength spectrum of graphene SPs with different $E_F$, calculated by FEM (solid lines) and RCWA (blue circles).

FEM method, results calculated by rigorous coupled wave theory (RCWA) [41,42] (blue circles) are shown as well, where $E_F = 0.535$eV. For RCWA, 20 diffraction orders are used to ensure precision, and graphene is treated as a thin layer with refractive index $n_g = \sqrt{1 + i\sigma_0/(\omega\varepsilon_0 d_g)}$, where $d_g = 0.34$nm is thickness of the monolayer graphene. The highly tunable linear response of the graphene SPs, indicates that our following discussions can be easily extended to other wavelengths, by choosing appropriate $E_F$ without varying structure parameters.

Figure 1(b) shows the transverse electric field intensity distribution normalized by incident light, in one period of grating, (at 10$\mu$m) and $E_F = 0.535$eV. Graphene layer is marked by white dotted line. Apparently, the field distribution shows features of graphene SPs, where electric field is tightly confined around graphene which is closed to grating ridge. Along with the tight field confinement, 160 times near field enhancement is achieved. Combining large near field enhancement and large $\sigma_3$ of graphene, we are able to lower the threshold of bistability as discussed in the following.

To achieve bistability, operation wavelength should be detuned from the resonant wavelength. In Fig. 1(c) we choose $E_F = 0.535$eV, $\tau = 400$fs, the resonant wavelength is around 10$\mu$m with the transmittance about 6%. The operation wavelength is chosen to be 10.6$\mu$m, and the linear transmittance is about 90%. In Fig. 2(a), we show the nonlinear transmittance in wavelength spectrum, under different incident light intensities, i.e. $I_{in} = 2\varepsilon_0 c|E_{in}|^2$ where $E_{in}$ is transverse electric field of incident light. When the light intensity is low ($I_{in} = 0.5$MW/cm$^2$), transmittance resembles the linear one. As $I_{in}$ increases, the resonant wavelength is shifted to longer wavelengths, the line shape becomes asymmetric and the transmittance becomes steeper on the side closed to 10.6$\mu$m, these are typical effects of nonlinear refractive index. Before $I_{in}$ is increased to 20MW/cm$^2$, the transmittance at 10.6$\mu$m remains to be high (90%). When $I_{in} = 20$MW/cm$^2$, due to the effect of third-order nonlinearity, the transmittance drops suddenly to about 10%. This procedure indicates the existence of optical bistability. From the following results, this intensity,

Optics EXPRESS

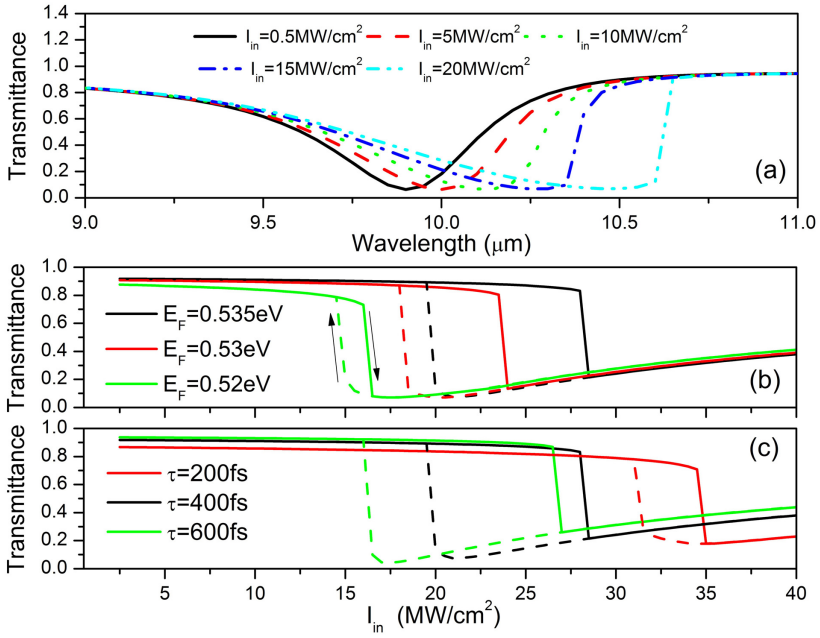


Fig. 2. (a) Nonlinear transmittance in wavelength spectrum with different $I_{in}$, $E_F$ = 0.535eV and $\tau$ = 400fs. (b) Dependence of transmittance on $I_{in}$ for different $E_F$, $\tau$ = 400fs. (c) Dependence of transmittance on $I_{in}$ for different $\tau$, $E_F$ = 0.535eV.

where the transmittance drops, predicts the lower threshold of bistability.

In Fig. 2(b), we show the bistability curves with different $E_F$. The curves are calculated in frequency domain using FEM method, scanning increased or decreased incident light intensity. During the calculation, the next result (field distribution), with larger/smaller intensity, is always calculated using the previous result, with smaller/larger intensity as initial conditions. Therefor, the fact that nonlinear responses are always related to field of previous time is simulated in frequency domain. This procedure is equivalent to calculations using FDTD method [11] in time domain, where calculations are done using incident light with a staircase function. In Fig. 2(b), 2(c), solid lines are calculated with an increased $I_{in}$, and dashed lines are calculated with a decreased $I_{in}$ (marked by the arrows). It is shown clear bistable behavior can be observed for all cases. For $E_F$ = 0.535eV, the lower switching-up threshold is about 20MW/cm$^2$ and the higher switching-down threshold is about 28MW/cm$^2$. We can decrease the thresholds by reducing $E_F$ slightly, the transmittance of high state is also decreased by a little. This can be understood qualitatively, if we reduce $E_F$ slightly, the resonant wavelength red shifts by a little, as a result the detuning between operation and resonant wavelength decreases. So lower intensity is needed to reduce transmittance at operation wavelength, as shown in Fig. 2(a). The threshold can be decreased to 15MW/cm$^2$ if $E_F$ = 0.52eV is used. In Fig. 2(c), the influence of the relaxation time of the carriers is also shown. It is known that $\tau$ is related to the intrinsic loss of graphene, and larger $\tau$ imply lower loss. As shown in Fig. 2(c), bistability with larger $\tau$ has a lower threshold, e.g. at $\tau$ = 600fs the threshold is decreased to 17MW/cm$^2$, and for $\tau$ = 200fs the threshold is increased to 32MW/cm$^2$.

The response time of the bistability is also calculated in time domain using FEM method. For the time domain FEM, we use time step of 1fs to keep accuracy. And resonable mesh size should be chosen to get stable results and decrease runtime. In the calculations, first $I_{in}$ is set slightly below switching-down (higher) threshold, after the transmitted intensity ($I_{out}$) is stable,

Optics EXPRESS

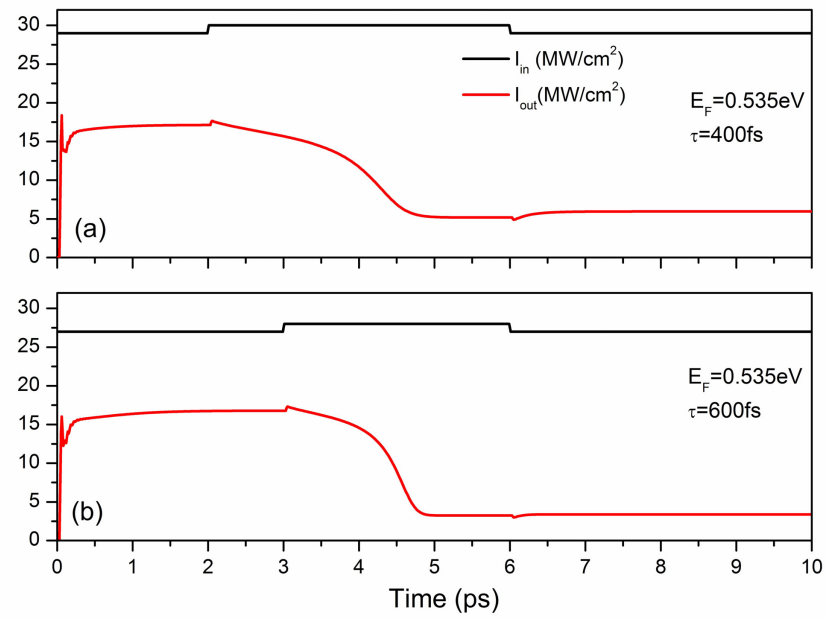


Fig. 3. Temporal response of bistability using (a)$E_F$ = 0.535eV, $\tau$ = 400fs (b)$E_F$ = 0.535eV, $\tau$ = 600fs.

the $I_{in}$ is increased just above the threshold, keep it a while and decrease $I_{in}$ to its original value. In short, the incident light is set to be a squire pulse. As shown in Fig. 3, the black lines are $I_{in}$ and the red lines are $I_{out}$, the overshoot and oscillatory behavior of $I_{out}$ in the beginning may due to the way of calculation. The increase of $I_{in}$ occurs at 2ps in Fig. 3(a) and 3ps in Fig. 3(b), as expected an increase of $I_{out}$ is observed at the same time, due to the fact that the nonlinear response is related to field of a former time. Afterward, $I_{out}$ decreases smoothly until a steady state corresponds to lower state of bistability. At 6ps, $I_{in}$ return to its original value, while $I_{out}$ remains to be low. This is a typical effect of bistability. From Fig. 3(a), for $E_F$ = 0.535eV, $\tau$ = 400fs, the response time is about 3ps. When $\tau$ is increased to 600fs, the response time is decreased to about 1.7ps. Note that the time delay of the nonlinear graphene is not considered in the calculations, the response time discussed above is only determined by the feedback of the structure [14]. However the nonlinear response time of graphene is less than 1ps [29], which is shorter than the response time of the proposed structure.

A disadvantage of the bistability using graphene SPs that excited by prism coupling, as in our previous studies [30], is that the resonances are quite angular sensitive. In practice, the divergence of incident optical beam is unavoidable, and the resonances can be significantly attenuated. The large angular dependence of the resonances stems from the steep dispersion relation of graphene SPs. While in graphene SPs with grating coupling, the resonances with normal incident light, correspond to a large stop band [36]. Due to large stop band, the dispersion relation is quite flat. As a result, less angular sensitivity can be expected for graphene SPs excited by gratings, so as for the bistability. In Fig. 4(a), the angular dependence of linear transmittance at 10.6$\mu$m is shown with different $E_F$ and $\tau$ = 400fs. For $E_F$ = 0.535eV, the detuning between 10.6$\mu$m and resonant wavelength is large, and the linear transmittance remains to be high for more than 60 degrees. As $E_F$ decreases to 0.49eV, the detuning decreases, and transmittance changes slightly until more than 50 degrees. When $E_F$ is 0.47eV, the resonant wavelength becomes 10.6$\mu$m, where the transmittance should be most sensitive to incident angle. As it can be

Optics EXPRESS

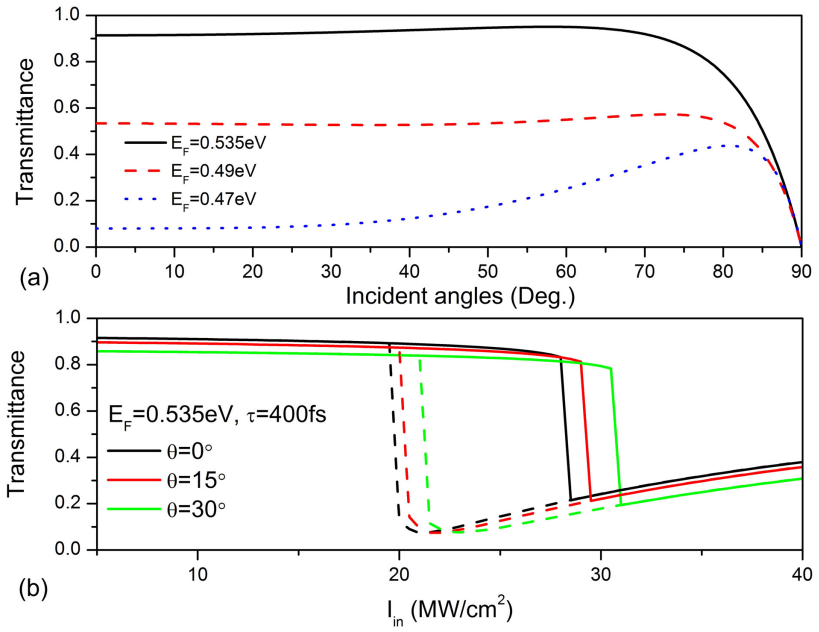


Fig. 4. (a)Angular dependence of linear transmittance with different $E_F$, and (b)Optical bistability with different incident angle.

seen, the transmittance is quite flat until 30 degrees. These results demonstrate that the linear transmittance is not sensitive to the incident angle. Fig. 4(b) shows the optical bistability with different incident angles. After the calculations, the bistability curve barely changes for angles smaller than 10 degree. While for $\theta = 15°$, the threshold changes less than 0.5MW/cm$^2$. Until $\theta = 30°$, the bistability curve start to be changed significantly, where the threshold changes by about 1.5MW/cm$^2$.

It is known that the graphene ribbons can support SPs, without requiring extra coupling method. There are similarities between SPs of graphene ribbons and graphene with gratings. The graphene ribbons can be treated like thin layer metal gratings. So in the following, SPs of graphene ribbons will be calculated, so as their bistabilities. The structure are shown in Fig. 5(a), where the graphene ribbons are placed on $CaF_2$ substrate. The period is $\Lambda = 1\mu$m, and the width of the graphene ribbons are $\Delta = 0.3\mu$m. In Fig. 5(b), the normalized transverse field intensity is shown with $\log_{10}$ scale in one period. The graphene ribbon is marked by dashed line. Note that at the same position there is the boundary between air and the substrate. As it is shown, the field enhancement is about $10^3$ at the center of ribbon, and reaches more than $10^3$ at the corner of ribbon. Such a large near field enhancement indicates a lower threshold of optical bistability. Fig 5(b) shows the nonlinear transmittance with different $I_{in}$, where $E_F$=0.21eV and $\tau$=400fs. For $I_{in}$ of less than 0.05MW/cm$^2$, the transmittance resembles linear ones. The black circles are linear transmittance calculated using RCWA method, with more than 60 diffraction orders are used. Similar to Fig. 2(a), as the intensity increases, the response becomes asymmetric. The sudden drop of the transmittance at 10.6$\mu$m occurs at $I_{in}$=0.75MW/cm$^2$, which is much lower than that in Fig. 2(a), indicating a much lower threshold of bistability.

Figure 6(a) shows optical bistability with $E_F$=0.21eV and different $\tau$. As it is shown, the threshold of bistability is about 0.5MW/cm$^2$ for $\tau = 600$fs, about 0.7MW/cm$^2$ for $\tau = 400$fs, and about 1.2MW/cm$^2$ for $\tau = 200$fs. These threshold are much lower than that in Fig. 2. Fig. 6(b) shows the temporal response of bistability with $E_F$=0.21eV and $\tau = 600$fs. As shown in

Optics EXPRESS

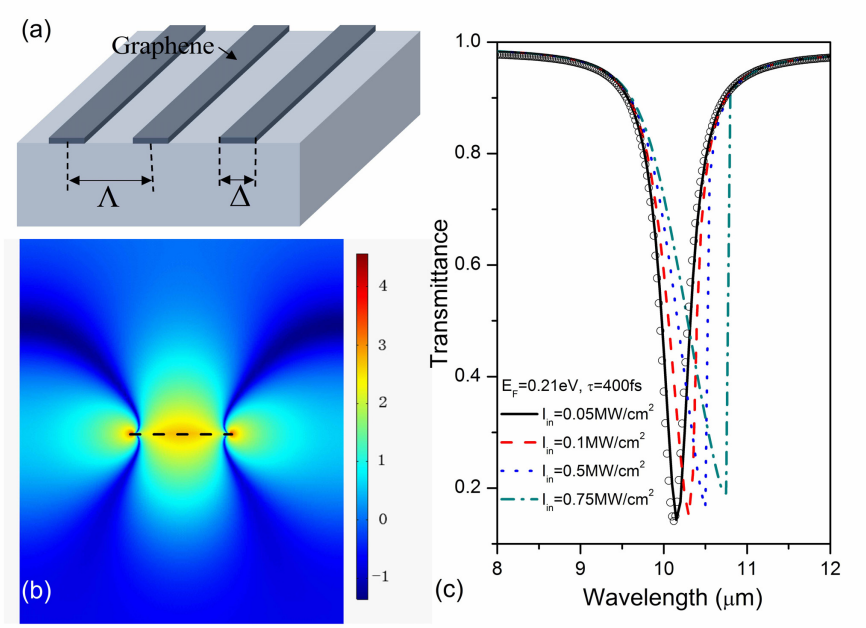


Fig. 5. (a) Schematic of the proposed structure. (b) Distribution of normalized electric filed intensity, with $\log_{10}$ scale, in one period. (c) Nonlinear transmittance in wavelength spectrum with different $I_{in}$.

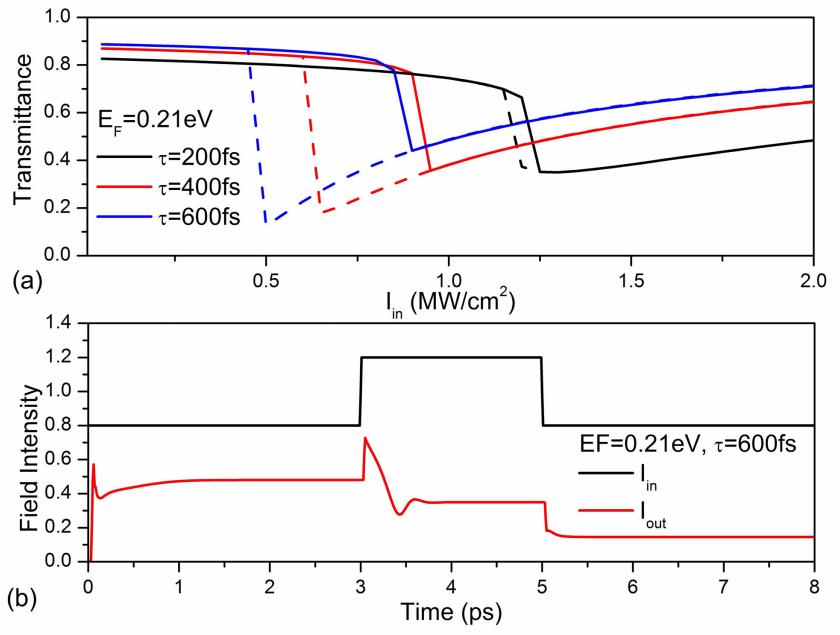


Fig. 6. (a) Optical bistability with different $\tau$. (b) Temporal response of bistability.

Optics EXPRESS

this figure, the response time is approximately 800fs, which is also shorter compared to Fig. 3. From the results, it can be concluded that regardless the complex fabrication, the graphene nanoribbons are more appropriate for bistable devices with low threshold and fast response time. Also the SPs of graphene ribbons are also angular insensitive, similar to that in Fig. 4.

## 4. Conclusion

In conclusion, in this work we have calculated the optical bistability of graphene SPs at mid-IR wavelength. The graphene SPs are excited by grating coupling with normal light incidence. Due to the large near field enhancement and large third-order nonlinear response of graphene, the achieved threshold of bistability is only about 20MW/cm$^2$. We also calculate the response time of the bistability. It is found that the response time can be shorten to about 1.7ps, and the angular insensitivity of our proposed structure is also demonstrated. In the end, we show the bistability based on SPs of graphene nanoribbons, which have similarities to metal gratings. Even lower threshold is demonstrated for the nanoribbons, which is only about 0.5MW/cm$^2$, and the response time can be further shorten to about 800fs. We believe that our results will be helpful for bistable devices fabrication and graphene SPs based all-optical switchings at mid-IR wavelengths to THz range.

## Funding

National Natural Science Foundation of China (Grant Nos. 61505111, 61490713 and 11647135); China Postdoctoral Science Foundation (Grant No. 2016M602509); the Guangdong Natural Science Foundation (Grant No. 2015A030313549); the Science and Technology Planning Project of Guangdong Province (Grant No. 2016B050501005); and the Science and Technology Project of Shenzhen (grant No. JCYJ20150324141711667).